Preparation and Characterization of Thermoplastic Polyurethane–Urea and Carboxylated Acrylonitrile Butadiene Rubber Blend Nanocomposites

Nasir Mahmood,[1,2] Asad Ullah Khan,[1] Zulfiqar Ali,[1] Mohammad Sohail Khan,[3] Anwar-Ul Haq,[1] Klaus Werner Stöckelhuber,[2] Uwe Gohs,[2] Gert Heinrich[2,4]

[1]*Department of Chemical Engineering, COMSATS Institute of Information Technology Defence Road off Raiwind Road, 54000 Lahore, Pakistan*
[2]*Leibniz-Institute of Polymer Research Dresden, Hohe Str. 6, D-01069 Dresden, Germany*
[3]*Federal-Mogul, Sealing Systems GmbH, Sales and Engineering Center Europe, D-51388 Burscheid, Germany*
[4]*Technische Universität Dresden, Institut für Werkstoffwissenschaft, D-01069 Dresden, Germany*

Received 20 January 2011; accepted 30 May 2011
DOI 10.1002/app.35008
Published online 22 September 2011 in Wiley Online Library (wileyonlinelibrary.com).

ABSTRACT: This study deals with the preparation and characterization of novel thermoplastic polyurethane–urea (TPUU) and carboxylated acrylonitrile butadiene rubber (XNBR) blends. Blends of different compositions were prepared in tetrahydrofuran using a solution technique, following an ultra-sonication. The chemical reaction between the two inherently immiscible blend phases was determined with the help of Fourier transform infrared-attenuated total reflectance (FTIR-ATR) spectroscopy and ^{1}H-nuclear magnetic resonance (^{1}H-NMR) spectroscopy. The identification of the new peaks in the FTIR-ATR spectra corroborates the existence of chemical reaction between the carboxylic functional group of XNBR and the amide group of the TPUU. In addition, an increase in the network crosslink density of the blend investigated using ^{1}H-NMR spectroscopy further supports the occurrence of the chemical reaction between the XNBR and the TPUU. The scanning and transmission electron micrographs of the blend morphology show a uniform dispersion of the minor TPUU phase in the XNBR. Furthermore, the existence of a single glass transition peak also confirms the enhancement in the interfacial miscibility. Additionally, the incorporation of 5 wt % of organomodified montmorillonite nanoclay improves the mechanical properties to a considerable extent in comparison with the unfilled blend elastomeric material. © 2011 Wiley Periodicals, Inc. J Appl Polym Sci 123: 3635–3643, 2012

Key words: blends; nanocomposites; ^{1}H-NMR; carboxylated acrylonitrile butadiene rubber; polyurethane–urea

INTRODUCTION

Polyurethane–ureas (PUU) are the segmented block copolymers with alternating soft and hard blocks. In the bulk phase, these two blocks separate into two different phases due to morphological differences.[1,2] The long chain diols form the soft segments (amorphous) and the hard segments (crystalline) are obtained from the reaction of a diisocyanate with a chain extender.[3–5] The chain extenders are either low molar mass diols or diamines. Such molecular combination of hard and soft segments provides unique properties to the TPUU. The hard segment (higher-modulus block) acts as physical crosslinks in the low-modulus soft phase, whereas the soft phase gives extensibility to the polymer.[6–8] The TPUU possess exceptional mechanical and chemical properties such as high tensile modulus, abrasion resistance, wear/tear resistance, chemical resistance, low-temperature elasticity, and ease of processing over other materials.[9] The practical applications are wide ranging in the automobile and aerospace industries; coatings; cable sheathing; and adhesives for textiles, leather, paper, and wood, etc.

There are numerous fundamental challenges which are associated with certain thermal and mechanical properties that are characteristic of the TPUU. The urethane/urea linkage is formed by a chemical bond between an isocyanate and a hydroxyl/amine group. This bond may break irreversibly under certain conditions. In some applications, such as automotive timing belts, V-belts, micro-ribbed belts, as well as other structures are subjected to repeated high- and low-temperature extreme dynamic-loading conditions. Polyurethane and polyurethane–urea elastomers have to-date been unacceptable for these long-term dynamic applications due to their tendency to wear and/or crack under these conditions.[10] The issues related to the thermal stability become more apparent for the

Correspondence to: N. Mahmood (nmahmood@ciitlahore.edu.pk).

TABLE I
Formulation of the Rubber Blend Mixes. Two Set of Samples Were used; One Set Containing 5% of Nanoclay of the XNBR+TPUU Contents, the Other Set Was Without Nanoclay

S. No	Rubber recipe	Amount [phr[a]]			
1	XNBR	100	90	80	70
2	TPUU	0	10	20	30
3	ZnO	3	2.7	2.4	2.1
4	*N*-Cyclohexyl-2-benzothiazolsulfanamide (CBS)	1.7	1.53	1.36	1.2
5	Stearic acid	2	1.8	1.6	1.4
6	Sulfur	1.4	1.26	1.12	0.98

[a] Parts per hundred of rubber.

high-temperature applications. This potential disadvantage limits the utilization of polyurethane and polyurethane–urea elastomers as high-performance material for engineering applications. This issue can partly be addressed through blending with other compatible components[11–13]. The blends vulcanizate thus produced can exhibit enhanced mechanical properties by prudent selection of the components[14–16]. The blending of the TPUU with carboxylated acrylonitrile butadiene rubber (XNBR) provides an alternative to explore for new multipurpose advance materials. The reported literature on the blends of polyurethane and acrylonitrile butadiene rubber (NBR) suggests that such a unique combination leads to an improved damping behavior, and as such, are potential candidates for vibration and sound-dampers.[17] In applications, such as gaskets, tubing pipes, coextrusion automotive gaskets, protective covers, automotive grips, ball pen grips, Desai et al. have reported that the NBR forms a disperse phase in PU rich matrix and vice versa. They have observed that an equal ratio blend results in a cocontinuous morphology due to the uniformly dispersed phases.[18]

The polymer–clay nanocomposite is one of the recent evolutionary steps in the polymer technology. A variety of clays and polymers have been successfully employed for the preparation of polymer nanocomposites. New synthesis routes, directly applicable in industry, have been the part of different studies.[19,20] The quality of the nanocomposites is characterized in terms of their enhanced mechanical properties, such as high stiffness, modulus, and their superior barrier properties.

In the present work, we report for the first time the preparation and characterization of the TPUU/XNBR blends and their clay nanocomposites. The amount of clay used was 5 wt % of the neat and blend samples. A variety of mechanical properties to validate the reinforcement ability of the nanoclay in such blend systems are discussed and compared with unfilled blends elastomeric material.

EXPERIMENTAL

Materials

Carboxylated acrylonitrile rubber (XNBR Krynac X 740) was received from Lanxess, Germany. Organomodified montmorillonite (Na-MMT) called nanofill 15 was supplied by Süd-Chemie AG, Germany. This clay contains quaternary ammonium salt as an organic modifier and the basal spacing of this organoclay is 2.98 nm. Zinc oxide, stearic acid, *n*-cyclohexyl-2-benzothiazole-sulfenamide (CBS), and soluble sulfur employed in this study were of industrial grades and used without any purification. Analytical grade tetrahydrofuran (THF) was received from ç-Aldrich and was used as such. The TPUU used in this study was synthesized by reacting 4,4′-diphenylmethane diisocyanates with a poly(tetramethylene carbonate)diol in presence of 1,2-di(*p*-aminophenoxy) ethane as chain extender. The reactants for preparing the TPUU were obtained from ç-Aldrich.

Preparation of TPUU and XNBR blends

The rubber blends and the blend nanocomposites were prepared by a two-step method. The formulation details are provided in Table I. In the first step, the TPUU and XNBR were dissolved in THF to obtain a homogenous mixture. The dissolved components were further blended at a temperature of 50°C for a period of 2 h in an ultra-sonication bath. Nanoclay-filled blend nanocomposites were prepared by adding 5 phr of nanofill 15 (organomodified montmorillonite) to the solution-mixture followed by ultra-sonication for enhanced dispersion. The mixture was then dried in a vacuum oven at 50°C for 12 h to ensure the complete removal of the THF. Finally, the additives such as zinc oxide, stearic acid, organic accelerators, and sulfur were added to the blend on a two-roll mixing mill. Curing studies were performed using a rubber processing analyzer Scarabaeus SIS V50 in an isothermal time-sweep mode at 150°C for 60 min. The final curing of

the blends was carried out at 150°C for 30 min in a compression molding machine.

Measurements

Fourier transforms infrared-attenuated total reflectance spectroscopy

The characterization of the interfacial compatibility of the blend phases was carried using the FTIR-ATR spectroscopy. The infrared spectra were recorded on a Vertex 80v (Bruker) FTIR spectrophotometer (4000–500 cm^{-1}, resolution 2 cm^{-1}, 32 scans per measurement) from Bruker Optik GmbH, Ettlingen, Germany. The spectra were taken in absorbance mode by placing the samples on the ATR cell.

^{1}H-Nuclear magnet resonance (NMR) spectroscopy

Pulsed ^{1}H-NMR spectroscopy (minispec mq20 NMR analyzer from Bruker, Germany) was used to determine relaxation behavior of different samples and to find insights about the impact of nano-scale heterogeneities of the materials onto the chain dynamics.

Differential scanning calorimetry analysis

The differential scanning calorimetric measurements were performed using a DSC analyzer Q1000, TA Instruments, USA, starting from −80 to 100°C in high-resolution mode with heating rate of 10 K/min under nitrogen atmosphere. The balance measurement accuracy was 0.1% and for the temperature calibration the well-known curie temperature of nickel standard sample was measured as a reference.

Dynamic mechanical thermal analysis

Dynamic mechanical thermal analysis was performed on the rectangle strips of dimensions 10 mm width and 35 mm length using a dynamic mechanical thermal spectrometer (Gabo Qualimeter, Germany, model Eplexor-150*N*) in the tension mode at a temperature range from −60 to 100°C. The isochronal frequency employed was 10 Hz and the heating rate was 2°K/min.

Scanning electron microscopy

Micro-structure morphology of the blends were determined with the help of LEO 435 scanning electron microscope (SEM – acceleration voltage 20 kV) manufactured by LEO Electron Microscopy Limited, Cambridge, England. Cryogenically fractured elastomeric composites were used for the dispersion analysis of the TPUU in the XNBR matrix.

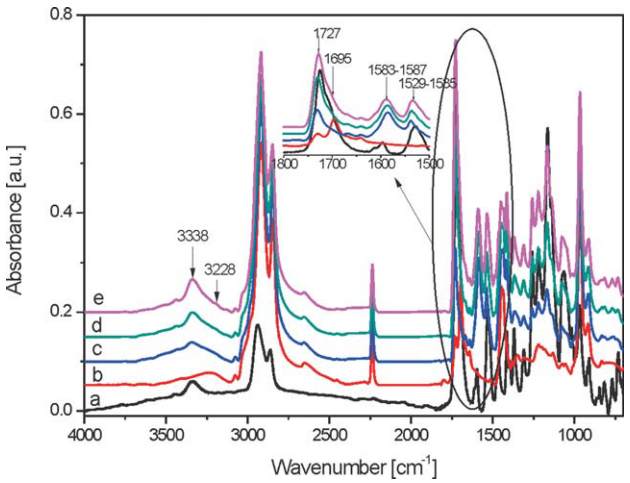

Figure 1 FTIR-ATR plots of (a) neat TPUU, (b) XNBR, and the blends containing XNBR:TPUU weight ratios: (c) 90 : 10 (d) 80 : 20, and (e) 70 : 30. [Color figure can be viewed in the online issue, which is available at wileyonlinelibrary.com.]

Transmission electron microscope

The high-resolution transmission electron microscope (HR-TEM) images were obtained on a JEOL 2100 transmission electron microscope. For the HR-TEM observation, ultrathin cross sections of the specimens were obtained at −80°C temperature in liquid nitrogen by using a Leica Ultra cut UCT ultramicrotome equipped with a diamond knife. The thickness of the HR-TEM specimens was approximately 80 nm. These specimens were then placed on the copper grid for the image analysis.

Mechanical properties

Stress–strain behavior of the TPUU/XNBR blends and the blend nanocomposites was determined according to ISO 527 method at a cross-head speed of 200 mm/min using a tensile testing machine from Zwick GmbH, Ulm Germany.

RESULTS AND DISCUSSION

Characterization of TPUU/XNBR blends

Figure 1 shows the FTIR-ATR spectra of the blends as well as their neat (pure) components. The functional group region (4000–1400 cm^{-1}) of the IR spectrum is used for the analysis rather than the fingerprint region (1400–500 cm^{-1}) which is complicated due to the skeletal vibrations of the polymer backbone. The neat TPUU shows distinct absorbance peaks at 1727 cm^{-1} (carbonate carbonyl), 1612 cm^{-1} (urethane carbonyl), 1596 cm^{-1} (urea carbonyl), and 1530 cm^{-1} (amide-II carbonyl), respectively. In the spectra for neat XNBR, the peaks corresponding to nitrile and the carboxylic group appear at 2224 and 1727 cm^{-1}, respectively. During processing, the –NH (i.e., urea and urethane –NH)

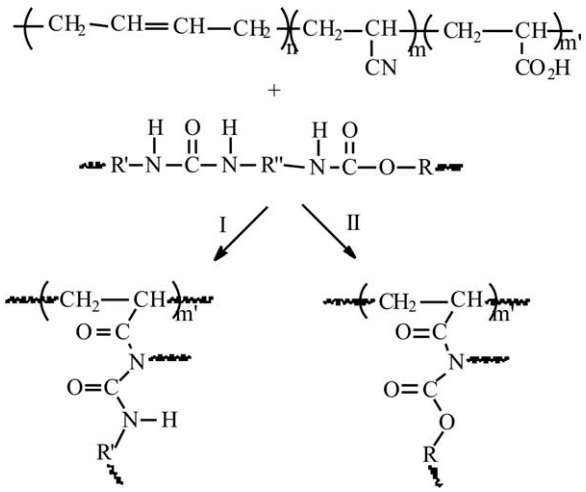

Scheme 1 Proposed chemical reaction between –NH and carboxylic group during blending of the TPUU and XNBR.

groups present on the TPUU backbone undergo a chemical reaction with the carboxylic group of the XNBR rubber leading to the formation of an amide bond (see Scheme 1). The urea –NH group in path-I and urethane –NH group in path-II of the scheme react with the carboxylic group present in the XNBR backbone. The increase in the intensity of the peak at 1585 and 1538 cm^{-1} is a clear indication of such a chemical reaction in all three blend compositions. Furthermore, in the case of neat XNBR there is no change in the absorption band at 2224 cm^{-1}. This is due to the stretching vibration of the nitrile group. The changes in the concentration of the nitrile group are not visible since the absorption is sharp and strong. The broad peak in the FTIR spectra in the range 3115–3455 cm^{-1} for pure XNBR has changed to a sharp bands appearing at 3342 cm^{-1}, for the blends. Such change in the FTIR spectra indicates the disappearance of the carboxylic hydroxyl group in the samples. These differences in the spectra of the XNBR and TPUU before and after blending are due to a chemical reaction between the –NH group and the carboxylic group.

^{1}H-NMR T_2 relaxation was measured for the neat and blend samples to investigate the influence of the different structural moieties on the chain dynamics. The T_2 relaxation time constants which are the characteristic of the different rates of the magnetization decay curve were determined by fitting the data into eq. (1). This equation has been successfully used to describe ^{1}H-NMR relaxometric behavior of many rubber/elastomer systems.[21] We note that recently developed double-quantum (DQ) NMR, which directly probes the restrictions of chain motions, can even provide more reliable information as ^{1}H-NMR relaxation methods[22–24]. However, for our studies ^{1}H-NMR T_2 relaxation yields sufficient information about a tentative impact of nano-scale heterogeneities of the investigated materials onto the chain dynamics:

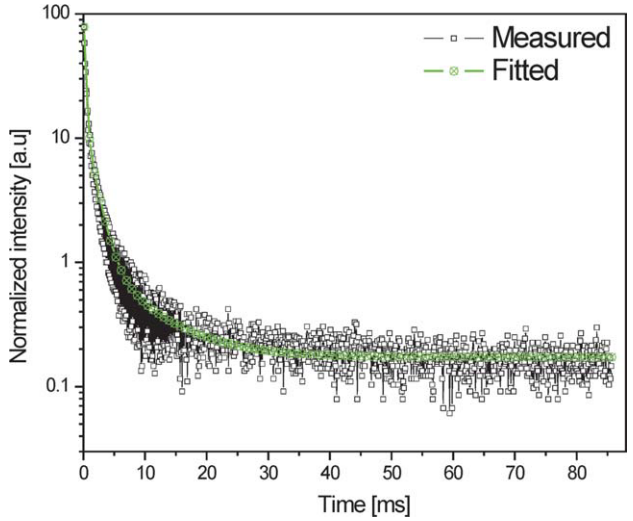

Figure 2 Plot showing the measured and the fitted T_2 relaxation time constant plot for the neat XNBR at 45°C. [Color figure can be viewed in the online issue, which is available at wileyonlinelibrary.com.]

$$A(t) = A_1(0)e^{\left(\frac{t}{T_{2f}}\right)^{\alpha}} + A_2(0)e^{\frac{t}{T_{2g}}} + A_3(0)e^{\frac{t}{T_{2c}}} \qquad (1)$$

The experimental data were fitted into the above equation by using Origin 8.0 (OriginLab Corp., Northampton, MA, USA). This package uses a nonlinear least-square fitting algorithm to fit the data. T_{2f}, T_{2g}, and T_{2c} are the relaxation time constants of the free chains, grafted chains, and crosslinked chains, respectively; α is a constant and a value of 1.35 has been suggested for systems similar to ones used in this study.[21] A_1, A_2, and A_3 are the relative amplitudes of the respective relaxation component.

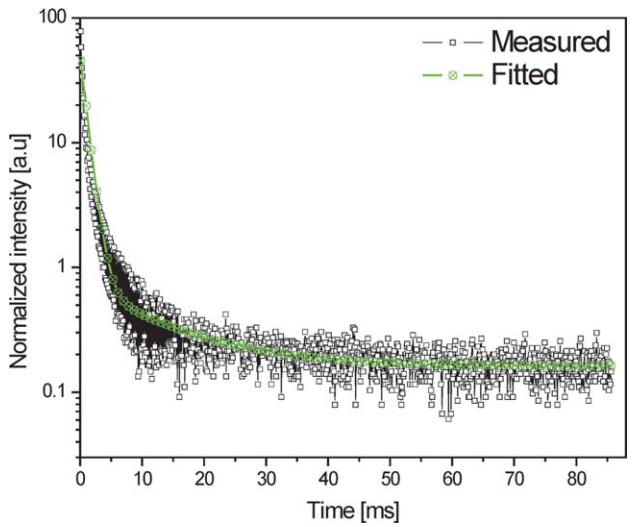

Figure 3 Plot showing the measured and the fitted T_2 relaxation time constant plot for the neat XNBR at 100°C. [Color figure can be viewed in the online issue, which is available at wileyonlinelibrary.com.]

TABLE II
^{1}H-NMR T_2 Relaxation Times for the Neat XNBR, Neat TPUU, and Their Blends as Measured at 45 and 100°C

Sample type	45°C			100°C		
	T_{2c}	T_{2g}	T_{2f}	T_{2c}	T_{2g}	T_{2f}
XNBR:TPUU (100:0)	0.22 ± 0.02	2.02 ± 0.04	7.80 ± 0.04	0.35 ± 0.01	2.36 ± 0.03	10.4 ± 0.02
XNBR:TPUU (90:10)	0.34 ± 0.03	1.79 ± 0.03	7.14 ± 0.02	0.38 ± 0.03	1.95 ± 0.05	7.87 ± 0.04
XNBR:TPUU (80:20)	0.33 ± 0.04	1.34 ± 0.05	5.40 ± 0.03	0.43 ± 0.02	2.15 ± 0.04	7.95 ± 0.08
XNBR:TPUU (70:30)	0.36 ± 0.03	1.87 ± 0.07	6.22 ± 0.04	0.40 ± 0.02	1.95 ± 0.07	7.88 ± 0.06
XNBR:TPUU (0:100)	0.65 ± 0.05	3.14 ± 0.04	14.11 ± 0.02	0.70 ± 0.05	3.10 ± 0.04	15.78 ± 0.07

The experimental data of the neat Xnbr are reported in Figures 2 and 3 at temperatures 45 and 100°C, respectively. The experimental data shown in the figures are in an average of four set of measurements carried out at the respective temperature. In the figures, a curve of the fitted parameters is also shown. Table II summarizes the relaxation time constants of the systems investigated in this study.

The results shown in Table II indicate that as the TPUU amount is decreased in the samples the value of T_{2c} also decreases at both the temperatures, i.e., 45 and 100°C. It suggests that there is a net effective increase in the crosslinking. This conclusion is based on the literature survey which states that if the crosslinking density decreases the value of T_{2c} relaxation constant increases.[25] The T_{2g} and T_{2f} values of all the samples investigated are also reported in Table II.

DSC measurements were carried out to explore the thermal behavior of the blends. Figure 4 shows the DSC thermograms of the TPUU, the XNBR, and the blends containing 10, 20, and 30 wt % of the TPUU. The second heating shows two distinct peaks for the TPUU and the blend samples. The exothermic peak at the higher temperature value is attributed to the melting (T_m) and the peak which is at the lower temperature is an endothermic one and is due to the crystallization (T_c). For the neat TPUU, the exothermic and the endothermic peaks appear at temperatures 41.3 and 19.5°C, respectively. The T_g of this sample is observed at a temperature of −35°C. For neat XNBR, no melting and crystallization is observed from the DSC results. However, it shows T_g at a temperature of −23°C. In the blended samples, the melting peaks appear at a temperature of 44.7°C, which is at a higher temperature as compared to the neat TPUU. Also the crystallization peaks for the blends are observed at a lower temperature, i.e., at −0.5°C when compared with the neat TPUU. The T_g of the blends is nearly constant and is very close to the T_g of neat XNBR. The data reported in Figure 4 show that the peak area increases as the amount of the TPUU is increased in the blends. The enthalpies of the different samples calculated from the DSC results are reported in Table III. The first enthalpy values in the table are representing per gram of the blend sample, whereas the second value is for per gram contents of the TPUU present in the blends. The existence of glass transition, melting, and crystallization properties in the TPUU is due to amorphous and crystalline morphology of it.

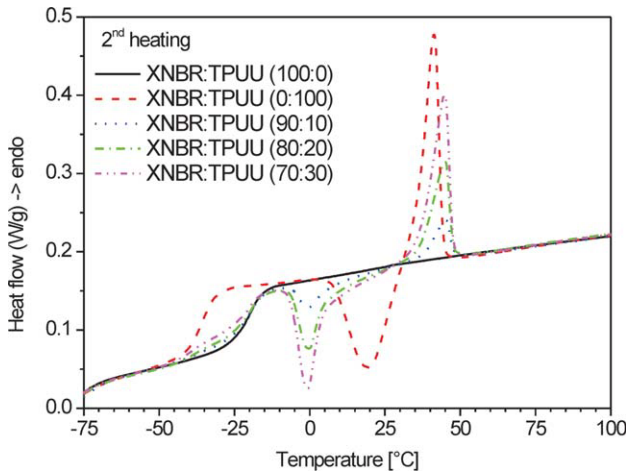

Figure 4 DSC plots of the neat XNBR, TPUU, and the blends containing XNBR:TPUU weight ratios, i.e., 90 : 10, 80 : 20, and 70 : 30. [Color figure can be viewed in the online issue, which is available at wileyonlinelibrary.com.]

For the blends, the FTIR results show that a chemical reaction is occurring between the urethane group of the TPUU and the carboxylic group in the XNBR (see Scheme 1). As a result of this reaction, the content of the crystalline part increases. This increase in the crystalline phase leads to an increase in the enthalpies of the blends. The existence of virtually a constant T_g for the blends indicates that the

TABLE III
DSC Data of the Neat XNBR, TPUU, and TPUU/XNBR Blends

S. No	Sample	ΔH_m (J/g)	ΔH_m (J/g $_{TPUU}$)
1	XNBR:TPUU (0:100)	34.8	34.8
2	XNBR:TPUU (100:0)	0.3	nil
3	XNBR:TPUU (90:10)	4.4	44
4	XNBR:TPUU (80:20)	9.4	47
5	XNBR:TPUU (70:30)	15.7	52

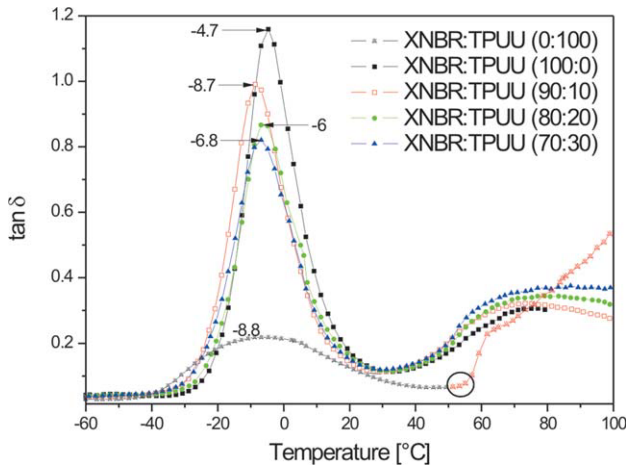

Figure 5 Temperature dependence of tan δ for the neat XNBR, TPUU, and the blends containing XNBR:TPUU weight ratios, i.e., 90 : 10, 80 : 20, and 70 : 30. [Color figure can be viewed in the online issue, which is available at wileyonlinelibrary.com.]

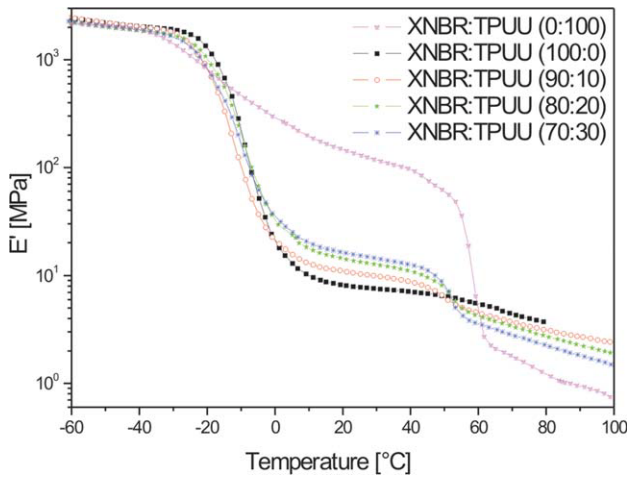

Figure 6 Temperature dependence of the storage moduli for the neat XNBR, TPUU, and the blends containing XNBR:TPUU weight ratios, i.e., 90 : 10, 80 : 20, and 70 : 30. [Color figure can be viewed in the online issue, which is available at wileyonlinelibrary.com.]

amorphous phases of the TPUU and XNBR are compatible.[26]

The dynamic mechanical thermal analysis (DMTA) traces depicted in Figures 5 and 6 display the storage modulus (E') and the loss factor (tan δ) as a function of temperature for the XNBR, the TPUU, and their corresponding blends. The TPUU has a glass transition temperature T_g at ca. −8.8°C, and a sharp shift of the loss factor at a temperature of 58°C. The later shift is probably due to the melting of the urethane and the urea hard segments. In the DSC results, the melting of these segments, i.e., the urethane and urea, was observed though at slightly lower temperature (refer to Fig. 4). The neat XNBR has a T_g at ∼ −4.7°C. In case of all the three XNBR/TPUU blend compositions, a single T_g at ca. −8.7, −6.7, and −6.8°C can be observed (Fig. 5). It also shows that with the increasing TPUU content, the peak height is decreased and also the T_g is shifted to middle value indicating the extent of miscibility of two phases. Interestingly, the melting of the hard segment phase of the TPUU is noticeably reduced in the XNBR/TPUU blends. This may be due to the effect of the chemical reaction between –COOH (XNBR) and –OH/NH (TPUU), which is disturbing the crystallization of the hard segments in the TPUU. The storage modulus below the T_g of the TPUU is in the same range for all the investigated samples. The storage modulus increases with the increasing the amount of the TPUU. When more TPUU is incorporated in the XNBR the storage modulus becomes higher. It is important to note that above a temperature of 55°C the storage modulus of the XNBR/TPUU blends is even smaller than that of the neat XNBR. At this transition, the mobility of the TPUU segments increases, possibly due to the melting of the hard segments in the TPUU. The DMTA response suggests that XNBR is the continuous phase (matrix) even in the blend with 30 wt % of the TPUU.

SEM image analyses were conducted on XNBR-gum and the blends containing different wt % of the TPUU to examine the phase morphology. The images acquired from the neat XNBR and a blend

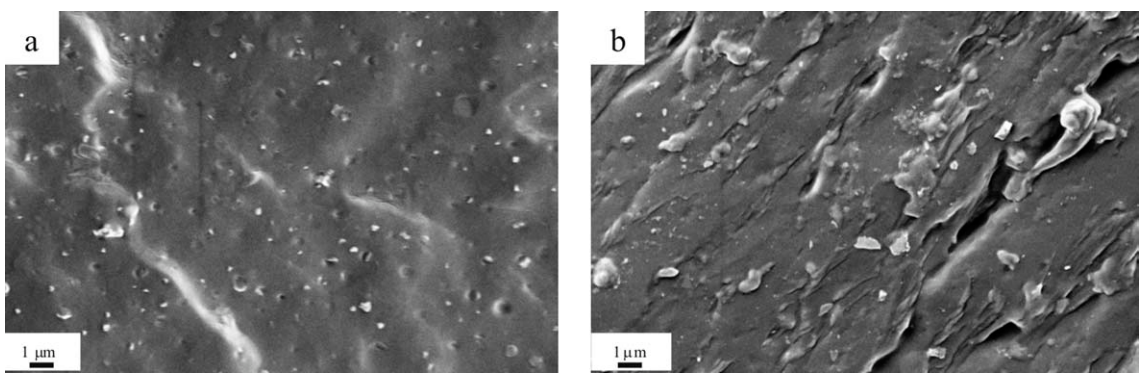

Figure 7 SEM images of (a) the neat XNBR and (b) the blend containing 80 : 20 (XNBR:TPUU).

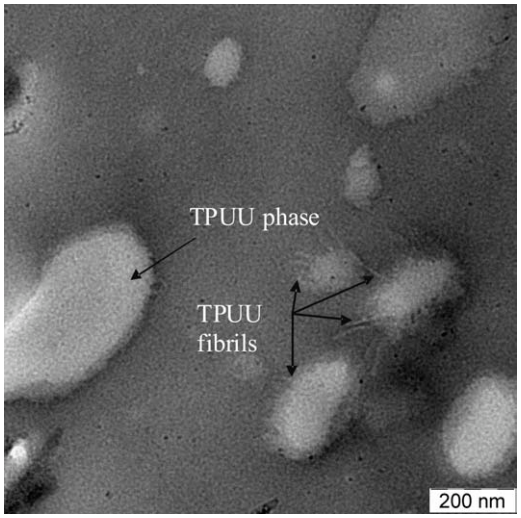

Figure 8 TEM image of a blend containing 80 : 20 (XNBR:TPUU).

containing 20 wt % of the TPUU are shown in Figure 7. The bright regions represent the curatives and the other ingredients contained in a typical rubber formulation [Fig. 7(a)]. In Figure 7(b), the image of XNBR/TPUU blend is shown. A rough and patterned surface can be observed from the image. This indicates that the TPUU and XNBR adhere strongly, which results from a chemical reaction between them.

Furthermore, a detailed overview of the blend phases can be observed from the TEM image shown in Figure 8, where a strong adhesion between the XNBR and TPUU can be observed. The TPUU phase is embedded in the rubber matrix, an indication of the enhanced compatibility. Moreover, the TPUU forms a fibril-like structure in the XNBR matrix. Such a network structure is formed as a result of a chemical reaction between urethane/urea –NH groups and the carboxylic group of the XNBR.

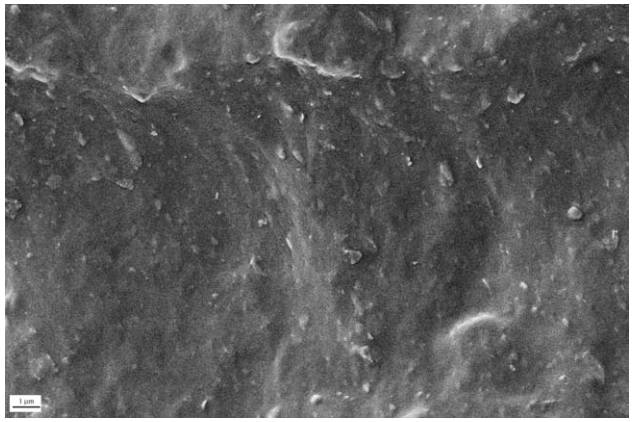

Figure 9 SEM images of the nanoclay filled 80 : 20 (XNBR:TPUU) blend sample. The amount of nanoclay used was 5 phr.

Characterization of the TPUU/XNBR blend nanocomposites

Figure 9 shows cryo-fractured surface SEM micrographs of a nanoclay-filled TPUU/XNBR blend. As discussed above, a rough and patterned surface can be observed in the unfilled blend image [Fig. 7(b)]. However, in the clay-filled blend a much finer phase structure is visible (Fig. 9). This result might be attributed to the homogenous dispersion of the clay into the blend.

Transmission electron microscopy (TEM) in contrast to the other techniques is a more direct one to observe the distribution of the clay in nanocomposites. The TEM images at different magnifications for a blend containing 5 phr of the nanoclay are shown in Figure 10(a,b). The low-magnification image shows the distribution of clay in the TPUU/XNBR matrix. The clay is homogeneously dispersed, although there remain few aggregates in the matrix. It is observed that the polymers infiltrate into the

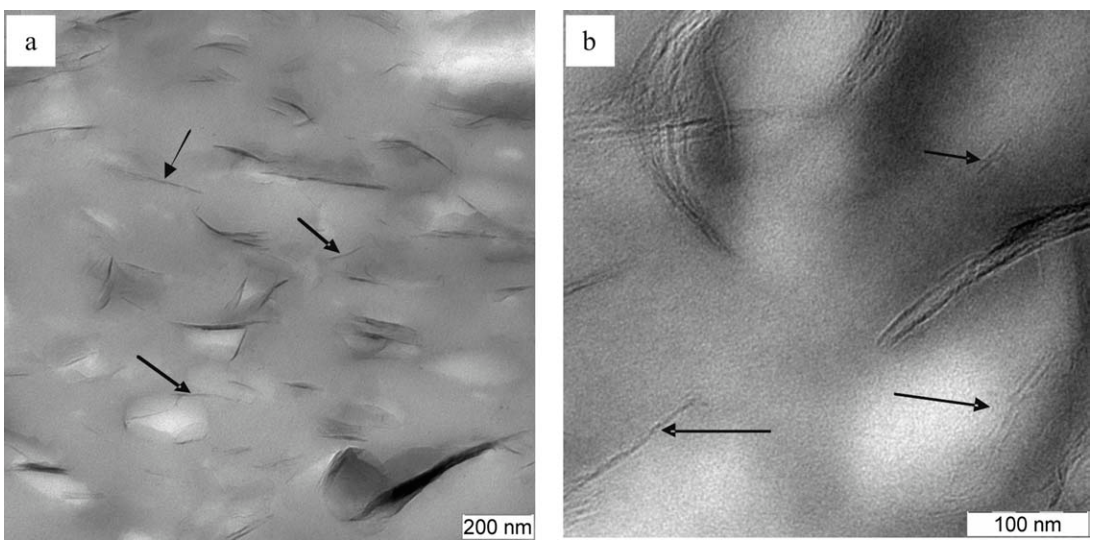

Figure 10 TEM images of nanoclay filled 80 : 20 (XNBR:TPUU) blend. The amount of nanoclay used was 5 phr.

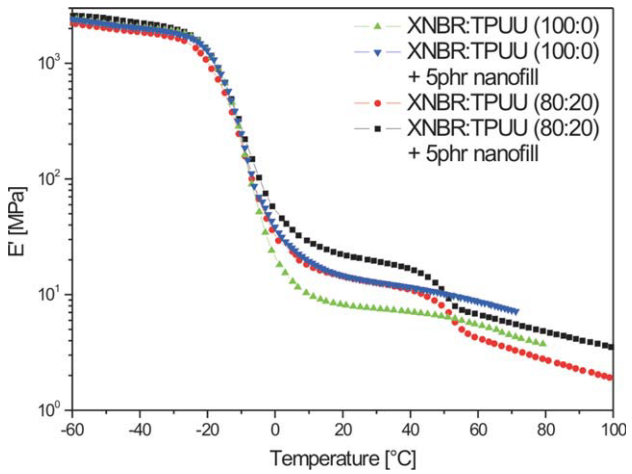

Figure 11 Storage moduli (E') of the unfilled and nanoclay-filled samples. [Color figure can be viewed in the online issue, which is available at wileyonlinelibrary.com.]

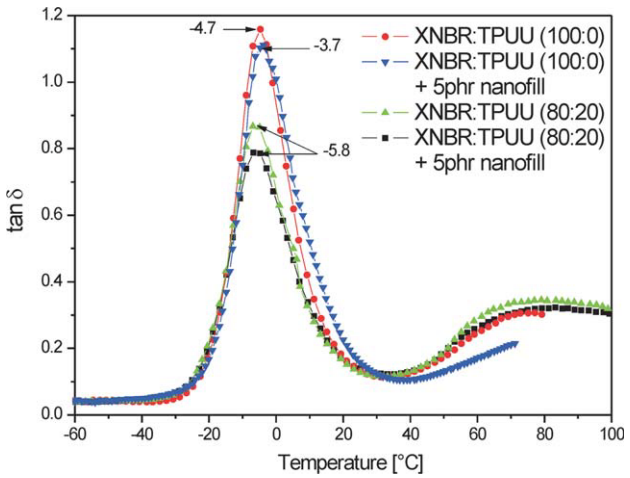

Figure 12 Temperature versus tan δ plots for the unfilled and nanoclay-filled samples. [Color figure can be viewed in the online issue, which is available at wileyonlinelibrary.com.]

clay layers but the ordered structure remains intact. In addition to the intercalated structure, in some spots, an exfoliated structure is also visible [Fig. 10(b)]. The clay is dispersed uniformly in the polymer matrix and not uniquely aligned. The SEM and TEM analyses confirm the formation of the newly developed TPUU/XNBR blend nanocomposites.

Figures 11 and 12 show the temperature dependencies of the storage moduli (E') and the loss factor (tan δ) of the filled blend nanocomposites. Figure 11 illustrates that storage moduli decrease with increasing temperature. This behavior is associated with the glass transition phenomenon occurring in elastomers. Above the room temperature, storage moduli increase with the increasing the amount of the TPUU. As can be seen in Figure 12, the glass transition temperature does not shift with the incorporation of the clay in the rubber matrix. However, the value of tan δ reduces considerably in the blend samples, which happens due to the confined mobility of the polymer chains. Therefore, the reduction in the tan δ value is an indication of increase in the mechanical properties such as elastic moduli.[27]

Table IV lists the mechanical properties of the TPUU/XNBR blends and their corresponding blend nanocomposite. The addition of the TPUU causes an enhancement of the mechanical properties of the TPUU/XNBR blends. It shows that the values of the moduli and elongation at break for these blends increases. This could be due to the chemical reaction between the –NH of urethane/urea and the –COOH group of the XNBR. Probably, the well-mixed and compatible TPUU phase in the XNBR efficiently transfers stress from the elastomer phase and improves the mechanical stiffness of the corresponding blend. These experimental results clearly indicate that the chemical structure introduced into the TPUU elastomers makes significant changes in its mechanical properties.

The results reported in Table IV also show that the addition of 5 wt % of nanoclay improves the mechanical properties to a significant level in comparison with their corresponding blends. On increasing the TPUU content, the desired mechanical properties increased for all the filled blend compositions. In general, an increase in the tensile strength accompanied by a decrease in the elongation is observed. However, in the TPUU/XNBR nanoclay-filled blend composites, the tensile strength increased in contrast to their corresponding blends (unfilled).

CONCLUSIONS

In conclusion, a series of the XNBR/TPUU blends containing different weight compositions of the TPUU were prepared and characterized. The

TABLE IV
Mechanical Properties: "Elastic Modulus (E_t), Stress (σ), Stress at Break (σ_B), Strain at Break (ε_B)," of Thermoplastic Polyurethane–Urea and Carboxylated Nitrile Butadiene Rubber Blends; 5% Clay Was Present in the Filled Samples

Sample type	Unfilled samples				Nanoclay-filled samples			
	E_t (MPa)	σ 300% (MPa)	σ_B (MPa)	ε_B (%)	E_t (MPa)	σ 300% (MPa)	σ_B (MPa)	ε_B (%)
XNBR:TPUU (100:0)	5.38 ± 0.25	2.71 ± 0.30	28.78 ± 1.86	1168 ± 80	6.90 ± 0.30	2.83 ± 0.15	29.50 ± 1.25	1140 ± 60
XNBR:TPUU (90:10)	7.02 ± 0.24	2.82 ± 0.37	25.0 ± 1.6	1206 ± 100	9.12 ± 0.87	3.67 ± 0.14	29.52 ± 2.14	1153 ± 35
XNBR:TPUU (80:20)	9.67 ± 0.48	3.04 ± 0.11	25.38 ± 2.5	1273 ± 80	11.43 ± 0.46	3.57 ± 0.16	31.77 ± 2.5	1279 ± 100
XNBR:TPUU (70:30)	10.77 ± 0.20	3.14 ± 0.27	22.94 ± 3.5	1260 ± 85	14.25 ± 1.19	3.83 ± 0.11	30.35 ± 1.95	1297 ± 80

absorption peak in the FTIR-ATR spectra at wavenumber 1585 and 1538 cm^{-1}, shows that the TPUU reacts chemically with XNBR. A single melting and crystallization peaks observed in DSC thermograms confirm the same backbone structure of the matrix, containing the TPUU and XNBR phases. In comparison with the pure XNBR, the corresponding TPUU/XNBR blends show enhanced mechanical properties due to the effect of the characteristic chemical reaction, enhanced interfacial compatibility, and increased crosslinking density in the TPUU elastomer. Furthermore, a significant improvement in the mechanical properties was achieved in the blends filled with nanoclay in comparison with the unfilled blends.

Financial and research support by the Leibniz Institute of Polymer Research, Dresden, is gratefully acknowledged.

References

1. Chu, B.; Gao, T.; Li, Y. J.;; Wang, J.; Desper, C. R.; Byrne, C. A. Macromolecules 1992, 25, 5724.
2. Li, Y. J.; Gao, T.; Liu, J.; Linliu, K.; Desper, C. R.; Chu B. Macromolecules 1992, 25, 7365.
3. Petrovic, Z. S.; Ferguson, J. Prog Polym Sci 1991, 16, 695.
4. Koberstein, J. T.; Stein, R. S. J Polym Sci Polym Phys 1983, 21, 1439.
5. Li, Y. J.; Gao, T.; Chu, B. Macromolecules 1992, 25, 1737.
6. Sarva, S. S.; Deschanel, S.; Boyce, M. C.; Chen, W. N. Polymer 2007, 48, 2208.
7. Sarva, S. S.; Hsieh, A. J. Polymer 2009, 50, 3007.
8. Hernandez, R.; Weksler, J.; Padsalgikar, A.; Choi, T.; Angelo, E.; Lin, J. S.; Xu, L. C.; Siedlecki, C. A.; Runt, J. Macromolecules 2008, 41, 9767.
9. Oertel, G, Ed., Polyurethane Handbook; Hanser Publishers: Munich, Germany, 1989.
10. Wu, W. W. L.; Stamp, J. R.; Brothers, W. J, US Patent No 6964626, 2005
11. Bruning, I.; Chlosta, A.; Scholz, G, US Patent No 6319985, 2001.
12. Tan, K. H.; Greef, J. L.; -de, US Patent No 4251642, 1981.
13. Haponiuk, J. T.; Balas, A. J Therm Anal 1995, 43, 211.
14. Naskar, N.; Debnath, S. C.; Basu, D. K. J Appl Polym Sci 2001, 80, 1725.
15. Abraham, T.; Sabet, A.; Ouhadi, T.; Barber, N., US Patent No 6207752, 2001.
16. Vogt, U.; Werneis, W.; Schuhmacher, G., US Patent No 5376723, 1994.
17. Kotal, M.; Srivastava, S. K.; Bhowmick, A. K. Polym Int 2010, 59, 2.
18. Desai, S.; Thakore, I. M.; Brennan, A.; Devi, S. J Macromol Sci A 2001, 38, 711.
19. Wells, L. A.; Cassidy, P. E.; Aminabhavi, T. M. A.; Perry, R. B. Rubber Chem Technol 1990, 63, 66.
20. Camberlin, Y.; Petrovic, J. P. J Polym Sci Polym Phys 1984, 22, 1835.
21. ten Brinke, J. W.; Litvinov, V. M.; Wijnhoven, J. E. G. J.; Noordermeer, J. W. M. Macromolecules 2002, 35, 10026.
22. Graf, R.; Demco, D. E.; Hafner, S.; Spiess, H. W. J Chem Phys 1997, 106, 885.
23. Litvinov, V. M. Macromolecules 2006, 39, 8727.
24. Saalwächter, K. Prog Nucl Magn Res Spectr 2007, 51, 1.
25. Sotta, P.; Fulber, C.; Demco, D. E.; Blümich, B.; Spiess, H. W.; Macromolecules 1996, 29, 6222.
26. Xiu, M. Q.; Jia W. X.; Xiao H. Y.; Xin L. W.; Zhen Z. J Appl Polym Sci 2007, 104, 3554.
27. Sharifi, S.; Kamali, M.; Mohtaram, N. K.; Shokrgozar, M. A.; Rabiee, S. M.; Atai, M.; Imani, M.; Mirzadeh, H.; Polymer Advanced Technologies DOI: 10.1002/pat. 1553.